AIAA JOURNAL
Vol. 49, No. 7, July 2011

Hybrid Source Model for Predicting High-Speed Jet Noise

S. J. Leib*
Ohio Aerospace Institute, Cleveland, Ohio 44142
and
M. E. Goldstein†
NASA John H. Glenn Research Center at Lewis Field, Cleveland, Ohio 44135

DOI: 10.2514/1.J050707

This paper introduces a novel hybrid source model into an existing acoustic analogy approach to obtain improved predictions of the turbulent mixing noise from cold, round, subsonic, and supersonic jets. The model incorporates new features of the Reynolds stress autocovariance tensor components found in recent experiments. The model parameters are determined from a Reynolds-averaged Navier–Stokes flow solution and experimental data. It is shown that this model significantly improves the predictions relative to previous results, particularly at observer polar angles between 90 degrees to the jet axis and the peak noise direction, indicating the importance of properly modeling relatively subtle characteristics of the autocovariance functions. The results are used to infer the relative importance of individual terms that make up the formula for the acoustic spectrum as a function of jet Mach number, frequency, and observer location.

Nomenclature

$A_{\kappa l}$	=	amplitude function
$a_{m,l}$	=	series coefficients
C_{ijkl}	=	amplitude scaling for turbulence autocovariance components
c	=	sound speed
c_∞	=	ambient sound speed
D	=	nozzle diameter
D_1^m, D_τ^l	=	differential operators
$g^a_{\lambda\kappa}$	=	adjoint vector Green's function
H	=	Helmholtz number
$\mathcal{H}_{\lambda jkl}$	=	spectrum
$H_{\lambda j\kappa l}$	=	generalized Reynolds stress autocovariance spectrum
h	=	enthalpy
I_ω	=	acoustic spectrum
$\boldsymbol{k}$	=	wavenumber vector
k	=	turbulent kinetic energy
$\bar{k}_1$	=	frequency-dependent streamwise wavenumber
$\bar{k}_T$	=	frequency-dependent transverse wavenumber
L	=	streamwise length scale
l_i	=	characteristic length scale
$\hat{l}_i$	=	normalized characteristic length scale
$\bar{l}_i$	=	frequency-dependent length scale
$\tilde{l}$	=	length scale parameter
M	=	acoustic Mach number
M_a	=	jet acoustic Mach number
p	=	pressure
$R_{\lambda j\kappa l}$	=	generalized Reynolds stress autocovariance tensor
$R^M_{\lambda j\kappa l}$	=	moving-frame Reynolds stress autocovariance tensor
$\tilde{R}$	=	normalized fixed-frame spectrum
R	=	magnitude of normalized fixed-frame spectrum
S	=	eikonal
T	=	averaging time
t	=	time
U_c	=	convection velocity
$U_{\text{crit lay}}$	=	critical-layer velocity
V	=	source volume
$\boldsymbol{y}$	=	source location
v_i	=	velocity vector
v'_4	=	generalized enthalpy fluctuation, $=(\gamma-1)(h'+\frac{1}{2}v'^2)$
X	=	$\sqrt{\tilde{\eta}_1^2+\tilde{\beta}^2+\tilde{\xi}_1^2}$
$\boldsymbol{x}$	=	observer location
x_c	=	distance to end of potential core
Z	=	$\frac{1}{X}(\tilde{\eta}_1+\frac{l_1}{l_0}\tilde{\xi}_1)^2$
α	=	exponent
β, $\hat{\gamma}$	=	arbitrary functions of $\hat{\xi}_T$
$\tilde{\beta}$, $\tilde{\gamma}$	=	arbitrary functions of $\tilde{\xi}_T$
$\bar{\beta}$	=	arbitrary functions of $\bar{\xi}_T$
$\Gamma_{\lambda j}$	=	Fourier-transformed propagator
γ	=	specific heat ratio
$\gamma_{\lambda j}$	=	propagator
$\delta_{\lambda\kappa}$	=	Kronecker delta
ε	=	turbulence dissipation rate
$\varepsilon_{\lambda j,\sigma m}$	=	$\delta_{\lambda\sigma}\delta_{jm}-\frac{\gamma-1}{2}\delta_{\lambda j}\delta_{\sigma m}$
$\bar{\eta}_i$	=	separation vector normalized by frequency-dependent length scale
$\bar{\eta}_T$	=	magnitude of transverse separation vector component normalized by frequency-dependent length scale
$\boldsymbol{\eta}$	=	separation vector
λ	=	characteristic frequency scale
ξ_i	=	moving-frame separation vector
θ	=	polar angle measured from jet axis
$\Phi_{\lambda jkl}$	=	spectral tensor
$\Psi_{\lambda jkl}$	=	generalized Reynolds stress spectral tensor
ρ	=	density
τ	=	time delay
ω	=	radian frequency
$\tilde{\omega}$	=	normalized radian frequency

Subscripts

i, j, k, l	=	tensor indices $= 1, 2, 3$
T	=	transverse component

Received 15 June 2010; revision received 15 October 2010; accepted for publication 7 December 2010.

*Senior Scientist. Senior Member AIAA.
†Senior Technologist. Fellow AIAA.

λ, κ = tensor indices $= 1, 2, 3, 4$

Superscripts

a	=	adjoint
M	=	moving-frame function
$\bar{}$	=	time average
$'$	=	fluctuating quantity
$\tilde{}$	=	Favre average
$*$	=	complex conjugate
$\hat{}$	=	normalized variables
∇	=	gradient operator
$\|\|$	=	absolute value

I. Introduction

JET mixing noise continues to be the main contributor to overall aircraft noise on takeoff, despite significant increases in engine bypass ratios. The development of effective mixing-noise reduction technologies, therefore, continues to be a high priority for the commercial aircraft industry, and robust noise prediction techniques are an important tool for accomplishing this. Most of these methods are based on the acoustic analogy approach, introduced by Lighthill [1] over 50 years ago.

Subsequent development of this approach led to formulations, such as that of Lilley [2], which explicitly account for mean flow interaction effects. Current state-of-the-art jet noise prediction codes (such as the JeNo code; Khavaran et al. [3]) use Lilley's formulation along with empirical models for the source terms and Reynolds-averaged Navier–Stokes (RANS) solutions to obtain the mean flow and turbulent kinetic energy.

Goldstein and Leib [4] recently developed an acoustic analogy approach for predicting high-speed jet noise from information about the turbulence. They introduced a number of modeling approximations about the mean flow and turbulence to reduce the general (and exact) formulation of [5] to a form that can be used for practical noise predictions. The acoustic predictions in [4] are based on their equation 6.27, which was obtained from the general formula by assuming that: 1) the mean flow is weakly nonparallel, 2) the four-dimensional space-time spectrum of the Reynolds stress autocovariance (which is termed the spectral tensor in this paper) has the same tensorial structure as the corresponding zero-wave-number tensor, 3) the autocovariance tensor is consistent with the quasi-normality hypothesis and, finally, 4) the turbulence is axisymmetric in a statistical sense.

Goldstein and Leib [4] used the weakly nonparallel mean flow approximation to construct a uniformly valid composite solution for the adjoint Green's function which eliminates the critical-layer singularity that occurs in the leading order solution when the observation angle is close to the downstream jet axis in supersonic flows. They also accounted for a "detuned" critical layer that occurs near the jet centerline when the difference between the centerline velocity and the critical-layer velocity, $U_{\text{crit lay}} = c_\infty/\cos\theta$, where c_∞ is the ambient sound speed and θ the polar angle measured from the downstream jet axis, is of the order of the mean flow spread rate.

Goldstein and Leib [4] used a general, nonseparable (in space and time), functional form to represent the components of the Reynolds stress autocovariance tensor (in a reference frame moving with the convection speed of the turbulence). The model is flexible enough to account for long-range coherence effects and exhibits the cusp at zero time and streamwise spatial separation observed experimentally. Their predictions, which use experimental data and a RANS code to obtain the required information about the turbulence, were compared with acoustic measurements taken on the NASA John H. Glenn Research Center at Lewis Field Small Hot Jet Acoustic Rig (SHJAR) and good agreement was obtained over a range of Mach numbers at two different observation angles. Subsequent comparisons at intermediate angles, however, were less satisfactory. The problem was traced to the empirical formula used to model the independent components of the Reynolds stress autocovariance tensor, and pointed to the need to further refine this model.

A number of recent experimental studies provide information about the details of the Reynolds stress autocovariance tensor in turbulent jets that are relevant to noise source modeling. Harper–Bourne [6] measured the streamwise component of the Reynolds stress autocovariance tensor, and associated spectrum, in a low-speed jet and found that, when the spatial separation vector components are nondimensionalized by appropriate frequency-dependent length scales, the magnitude of the coherence (i.e., the spectrum normalized to unity at zero separation) becomes independent of frequency. Morris and Zaman [7,8] also measured the streamwise component of the Reynolds stress autocovariance tensor, as well as the amplitudes (zero space-time separation) of certain transverse components. Morris and Zaman [9] extended these measurements to include components of the Reynolds stress autocovariance tensor involving radial velocity fluctuations and the associated length scales.

These experiments provide well-resolved details of some of the quantities that need to be modeled in an acoustic analogy approach to jet noise but, owing to their use of hot-wire anemometry, are limited to relatively low Mach number, cold flows. An extensive database documenting the mean flow, turbulence and acoustics of turbulent jets over a wide range of operating conditions has been assembled from measurements taken on the SHJAR at NASA John H. Glenn Research Center at Lewis Field [10–13]. The measurements were taken with a particle imaging velocimeter (PIV) to study supersonic and hot flows. Prokora and McGurik [14] made PIV measurements in subsonic round jets.

The objective in [4] was to implement the exact acoustic analogy formulation in [5] using a minimum number of assumptions and approximations, and to base those which could not be avoided, as far as possible, on experimental data or results of numerical simulations. But Afsar et al. [15] and Afsar [16] have shown that some of the assumptions in [4] were unnecessary and, thereby, put the modeling approximations on a more rigorous theoretical basis. In particular, they show that it is only required to assume that the Reynolds stress autocovariance tensor depends on the transverse component of the spatial separation vector only through its magnitude, and that the resulting quantity is an axisymmteric tensor, to obtain the result used in [4]. Afsar et al. [15] refer to this as a statistical axisymmetric turbulence model, and we use that terminology here. Afsar [16] also obtained a slight generalization of equation 6.27 of [4] that applies even when assumption 1 is not satisfied, but we use this approximation in this paper to simplify the computations.

The statistically axisymmetric model for the Reynolds stress autocovariance was rigorously developed in Afsar et al. [15], making only the approximations described above, by decomposing this tensor into its basic invariants and using the pair symmetries implied by its definition. They compared this model with data from a large eddy simulation (LES) of a Mach 0.75 isothermal round jet. Their results show that the statistically axisymmetric turbulence model captures the correct spatial behavior of the invariants of the Reynolds stress autocovariance tensor.

The main purpose of using the statistically axisymmetric turbulence model is to reduce the large number of independent components of the Reynolds stress autocovariance tensor that appear in the formula for the acoustic spectrum down to a more manageable level, consistent with a practical jet noise prediction scheme. Its use was originally proposed (Goldstein and Rosenbaum [17]) as an alternative to the simpler, but less physically realistic, isotropic model for this purpose. Its use in acoustic analogy based jet noise predictions has been accepted for some time (beginning with Khavaran [18]) as providing a theoretically consistent way to represent the experimentally observed anisotropy in round turbulent jets with a relatively minimal amount of algebraic complexity. More recent experiments and numerical simulations have continued to provide support for use of this model in jet noise predictions.

One purpose of the present paper is to introduce a new, fixed-frame model for the space-time Fourier transform of the fluctuating Reynolds stress autocovariance tensor, which is more consistent with characteristics observed in recent experimental measurements of jet turbulence than the moving-frame model used in [4]. The model can be thought of as a hybrid between previous frequency-domain (with

frequency-dependent length scales) and time-domain approaches. This diminishes the role of source convection effects, which means that the predicted directionality of the radiated sound is now almost entirely due to mean flow interaction effects and retarded time variations across the source region. (It is now well known that the mean flow interactions can significantly amplify the small-angle sound radiation [19–21].) Another purpose of this paper is to extend the range of comparisons with data to improve the level of confidence in the predictions.

Section II summarizes the relevant parts of the acoustic analogy formulation of [5], and Sec. III introduces a model for the sound propagation/source interaction, which takes advantage of the disparity in length scales between the mean flow and the turbulence, to simplify the general result. Section IV, which describes the details of the new source model, shows that the suitably normalized spectrum of the autocovariance tensor becomes independent of frequency when appropriate frequency-dependent length scales are introduced as found experimentally by Harper–Bourne [6]. This result is used to improve the consistency of the model with the experimental measurements. The coefficients used in the source model are described in Sec. V where the resulting predictions are compared with data and the effects of the individual terms in the formula for the acoustic spectrum are discussed. The results show that relatively subtle changes in the long-range tails of the autocovariance functions can have a large effect on the shallow angle acoustic radiation at high Mach numbers. Finally, conclusions and comments on possible future work are made in Sec. VI.

II. Basic Equation

The Fourier transform

$$I_\omega(\boldsymbol{x}) \equiv \frac{1}{2\pi}\int_{-\infty}^{\infty} e^{i\omega\tau}\overline{p^2}(\boldsymbol{x},\tau)\,\mathrm{d}\tau \tag{1}$$

of the far-field pressure autocovariance

$$\overline{p^2}(\boldsymbol{x},\tau) = \lim_{T\to\infty}\frac{1}{2T}\int_{-T}^{T} p'(\boldsymbol{x},t)\,p'(\boldsymbol{x},t+\tau)\,\mathrm{d}t \tag{2}$$

(the acoustic spectrum at the observation point $\boldsymbol{x}$) can be expressed in terms of $I_\omega(\boldsymbol{x}|\boldsymbol{y})$, the acoustic spectrum at $\boldsymbol{x}$ due to a unit volume of turbulence at $\boldsymbol{y}$, by

$$I_\omega(\boldsymbol{x}) = \int_V I_\omega(\boldsymbol{x}|\boldsymbol{y})\,\mathrm{d}\boldsymbol{y} \tag{3}$$

where the integration volume, V, is the entire source region, $p' \equiv p - \bar{p}$ and overbars are being used to denote time averages. Goldstein and Leib [4] show that this latter quantity is given by

$$I_\omega(\boldsymbol{x}|\boldsymbol{y}) = (2\pi)^2\Gamma_{\lambda j}(\boldsymbol{x}|\boldsymbol{y};\omega)\int_V \Gamma^*_{\kappa l}(\boldsymbol{x}|\boldsymbol{y}+\boldsymbol{\eta};\omega)\mathcal{H}_{\lambda j\kappa l}(\boldsymbol{y},\boldsymbol{\eta},\omega)\,\mathrm{d}\boldsymbol{\eta} \tag{4}$$

where the asterisk denotes complex conjugates, the Greek indices range from one to four, and the Latin indices from one to three

$$\Gamma_{\lambda j} \equiv \frac{1}{2\pi}\int_{-\infty}^{\infty} e^{i\omega(t-\tau)}\gamma_{\lambda j}(\boldsymbol{x}|\boldsymbol{y},t-\tau)\,\mathrm{d}(t-\tau) \tag{5}$$

is the Fourier transform of a "propagator"

$$\gamma_{\lambda j}(\boldsymbol{x},t|\boldsymbol{y},\tau) \equiv \frac{\partial g^a_{\lambda 4}(\boldsymbol{y},\tau|\boldsymbol{x},t)}{\partial y_j} - (\gamma-1)\delta_{\lambda k}\frac{\partial \tilde{v}_k}{\partial y_j}g^a_{44}(\boldsymbol{y},\tau|\boldsymbol{x},t) \tag{6}$$

that depends on the fourth component of the adjoint vector Green's function $g^a_{\lambda\kappa}(\boldsymbol{y},\tau|\boldsymbol{x},t)$, which can be calculated from equations 4.8–4.11 of [4] once the mean flow is known.

The spectrum $\mathcal{H}_{\lambda j\kappa l}$ is related to the spectrum

$$H_{\lambda j\kappa l}(\boldsymbol{y},\boldsymbol{\eta},\omega) = \frac{1}{2\pi}\int_{-\infty}^{\infty} e^{-i\omega\tau}R_{\lambda j\kappa l}(\boldsymbol{y},\boldsymbol{\eta},\tau)\,\mathrm{d}\tau \tag{7}$$

of the generalized Reynolds stress autocovariance tensor

$$R_{\lambda j\kappa l}(\boldsymbol{y},\boldsymbol{\eta},\tau) \equiv \lim_{T\to\infty}\frac{1}{2T}\int_{-T}^{T}[\rho v'_\lambda v'_j - \overline{\rho v'_\lambda v'_j}](\boldsymbol{y},\tau_0)[\rho v'_\kappa v'_l - \overline{\rho v'_\kappa v'_l}](\boldsymbol{y}+\boldsymbol{\eta},\tau_0+\tau)\,\mathrm{d}\tau_0 \tag{8}$$

by the simple linear transformation

$$\mathcal{H}_{\lambda j\kappa l} = \varepsilon_{\lambda j,\sigma m}H_{\sigma m\gamma n}\varepsilon_{\kappa l,\gamma n} \tag{9}$$

where $v'_\lambda \equiv v_\lambda - \tilde{v}_\lambda$ denotes a generalized, four-dimensional "velocity" fluctuation, with v_i, $i = 1, 2, 3$, being the ordinary fluid velocity and $v'_4 \equiv (\gamma-1)(h' + \frac{1}{2}v'^2)$, where h' is the fluctuating enthalpy ([4]), $\tilde{v}_k$ denotes the Favre-averaged flow velocity, and

$$\varepsilon_{\lambda j,\sigma m} \equiv \delta_{\lambda\sigma}\delta_{jm} - \frac{\gamma-1}{2}\delta_{\lambda j}\delta_{\sigma m} \tag{10}$$

It is important to note that it would be impossible to define the Fourier transform (7) if the autocovariance tensor (8) were replaced by the correlation tensor

$$\lim_{T\to\infty}\frac{1}{2T}\int_{-T}^{T}\rho v'_\lambda v'_j(\boldsymbol{y},\tau_0)\rho v'_\kappa v'_l(\boldsymbol{y}+\boldsymbol{\eta},\tau_0+\tau)\,\mathrm{d}\tau_0 \tag{11}$$

as is frequently done in analyses based on a Lilley-type equation since, as pointed out by Batchelor [22], this latter quantity tends to a nonzero value as $\tau\to\infty$.

This result (which also serves as the basis of the analysis in [4]) shows that there is an exact relation between the quantities that are usually measured in aeroacoustics experiments, namely the far-field acoustic spectrum and the generalized Reynolds stress autocovariance tensor. It is completely general and applies to any localized turbulent flow, even in the presence of fixed solid surfaces, but is probably too complicated to use for routine jet noise predictions. The general results were used, along with a LES of the flowfield, to calculate the noise from a Mach 0.75 turbulent air jet [23,24], but the calculations are very time consuming.

III. Modeling Propagator/Turbulent Source Interaction

Significant simplification can be obtained if the propagator is taken outside of the integral over the separation vector in Eq. (4). But this amounts to neglecting variations of the Green's function over the turbulence correlation region, or neglecting so-called "retarded-time" effects. It is known that these effects can give rise to subtle source cancellations and that neglecting them can lead to errors in the noise predictions.

The velocity fluctuations in turbulent jets tend to be correlated over distances that are relatively short compared with the corresponding transverse and streamwise length scales of the mean flow, say D and L, respectively. Although the streamwise distances over which these fluctuations are correlated tend to be longer than the corresponding transverse ones, the mean flow varies much more slowly in the streamwise direction than the transverse direction in the high-Reynolds number flows of interest in jet noise applications. Measurements presented by Prokora and McGurik [14] provide evidence that the transverse correlation lengths are small relative to the transverse mean flow length scales. Based on these observations, we make the assumption here that the turbulence correlation lengths are short compared with the corresponding mean flow lengths and show that this disparity in length scales can be exploited to obtain a simplified formula for the acoustic spectrum which takes into account variations in retarded time in a systematic way.

Since the linear equation governing the far-field adjoint Green's function depends only on the mean flow and reduces to the wave equation outside the source region, the only length scales upon which this solution can depend are those of the mean flow (which enter through the coefficients of the equation), and the acoustic wavelength c_∞/ω (since only acoustic waves reach the far field). When all these length scales are large compared with the turbulence correlation

lengths, the adjoint Green's function (and therefore the propagator) will be relatively constant over the correlation region, and may therefore be moved outside the integral over the separation vector in Eq. (4). However, these variations cannot be neglected when any of these length scales is of the order of, or smaller than, the correlation length, which, in view of our assumption above, can only be c_∞/ω. To account for these variations in a self-consistent way, we note that the Helmholtz number $H = \omega D/c_\infty$ (which is the ratio of the transverse mean flow length scale to the acoustic wave length) must be large in this case and that $\Gamma^*_{\lambda l}(\boldsymbol{x}|\boldsymbol{z},\omega)$ can be represented by its high-frequency, or Wentzel, Kramers, Brillouin, and Jeffreys, approximation (see Acknowledgements for more information)

$$\Gamma^*_{\lambda l}(\boldsymbol{x}|\boldsymbol{z},\omega) \approx A_{\lambda l}(\boldsymbol{x}|\boldsymbol{z},\omega)\exp\left[i\frac{\omega}{c_\infty}S(\boldsymbol{x}|\boldsymbol{z})\right] \tag{12}$$

where $S(\boldsymbol{x}|\boldsymbol{z})$ satisfies the (adjoint) Eikonal equation

$$(\nabla_z S)\bullet(\nabla_z S) = [1-\boldsymbol{M}(\boldsymbol{z})\bullet\nabla_z S]^2 c_\infty^2/\widetilde{c^2} \tag{13}$$

where $\boldsymbol{M}(\boldsymbol{z}) \equiv \tilde{\boldsymbol{v}}/c_\infty$ is the acoustic Mach number at $\boldsymbol{z}$, and $A_{\lambda l}(\boldsymbol{x}|\boldsymbol{z},\omega)$ satisfies an appropriate transport equation and expands like

$$\frac{\omega}{c_\infty}A^{(0)}_{\lambda l}(\boldsymbol{x}|\boldsymbol{z}) + A^{(1)}_{\lambda l}(\boldsymbol{x}|\boldsymbol{z}) + \frac{c_\infty}{\omega}A^{(2)}_{\lambda l}(\boldsymbol{x}|\boldsymbol{z}) + \left(\frac{c_\infty}{\omega}\right)^2 A^{(3)}_{\lambda l}(\boldsymbol{x}|\boldsymbol{z}) + \ldots \tag{14}$$

Since both $A_{\lambda l}(\boldsymbol{x}|\boldsymbol{z},\omega)$ and $S(\boldsymbol{x}|\boldsymbol{z})$ depend only on the mean flow, their $\boldsymbol{z}$ variation must be on the scale of the mean flow.

Since we are making the assumption that the mean flow length scales are long compared with their corresponding correlation lengths, the Eikonal will be relatively constant over the integration variable in Eq. (4) and may be expanded in a Taylor series for variations on this scale to obtain

$$\Gamma^*_{\lambda l}(\boldsymbol{x}|\boldsymbol{y}+\boldsymbol{\eta},\omega) \approx \Gamma^*_{\lambda l}(\boldsymbol{x}|\boldsymbol{y},\omega)\exp\left[i\frac{\omega}{c_\infty}\boldsymbol{\eta}\cdot\nabla_y S(\boldsymbol{x}|\boldsymbol{y})\right] \tag{15}$$

This means that the formula (4), for the far-field spectrum can be written as

$$I_\omega(\boldsymbol{x}|\boldsymbol{y}) \approx (2\pi)^2\Gamma_{\lambda j}(\boldsymbol{x}|\boldsymbol{y};\omega)\Gamma^*_{\kappa l}(\boldsymbol{x}|\boldsymbol{y};\omega)\Phi^*_{\lambda j\kappa l}\left(\boldsymbol{y};\frac{\omega}{c_\infty}\nabla_y S,\omega\right) \quad \text{as } |\boldsymbol{x}|\to\infty \tag{16}$$

where the turbulence autocovariance tensor enters only through the spectral tensor

$$\Phi^*_{\lambda j\kappa l}(\boldsymbol{y};\boldsymbol{k},\omega) \equiv \int_V e^{i\boldsymbol{k}\bullet\boldsymbol{\eta}}\mathcal{H}_{\lambda j\kappa l}(\boldsymbol{y},\boldsymbol{\eta},\omega)\,\mathrm{d}\boldsymbol{\eta} \tag{17}$$

Note that this formula reduces to the result obtained by neglecting variations in the propagator over the integration volume when the acoustic wavelength is larger than the turbulence correlation length, so it is expected to provide a valid approximation at all wavelengths, as long as our basic assumption about the turbulence is satisfied. But it should provide a valid approximation even if it is not very well satisfied, for example if the turbulence length scales are of the order of the transverse mean flow length scale D, since it has been demonstrated [25] that the high-frequency approximation Eq. (12) tends to be very robust and remains reasonably accurate down to $\mathcal{O}(1)$ Helmholtz numbers.

For the nearly parallel mean flows of interest in jet noise problems $\Gamma^*_{\kappa l}(\boldsymbol{x}|\boldsymbol{y},\omega)$ behaves like

$$\Gamma^*_{\kappa l}(\boldsymbol{x}|\boldsymbol{y},\omega) \to \Gamma^*_{\kappa l}(\boldsymbol{x}|\boldsymbol{y}_T,\omega)\exp\left[i\frac{\omega}{c_\infty}y_1\cos\theta\right] \quad \text{as } |\boldsymbol{x}|\to\infty \tag{18}$$

where y_1 is in the mean flow direction, $\boldsymbol{y}_T \equiv \{y_2, y_3\}$ and θ is the polar angle measured from the y_1 axis. The streamwise component of the wavenumber vector, $\boldsymbol{k} = \omega\nabla_y S/c_\infty$, can therefore be reasonably well approximated by $(\omega/c_\infty)\cos\theta$ at all frequencies and the Eikonal Eq. (13) can then be approximated by the parallel flow Eikonal equation

$$(\nabla_{\boldsymbol{y}_T}S)\bullet(\nabla_{\boldsymbol{y}_T}S) = [1-M(\boldsymbol{y}_T)\cos\theta]^2 c_\infty^2/\widetilde{c^2} - \cos^2\theta \tag{19}$$

which means that only the transverse components, say $\boldsymbol{k}_T = \{k_2, k_3\}$, of $\boldsymbol{k}$ have to be calculated in this case.

The statistically axisymmetric turbulence approximation implies that $R_{ijkl}(\boldsymbol{y},\eta_1,\boldsymbol{\eta}_T,\tau) \approx R_{ijkl}(\boldsymbol{y},\eta_1,\eta_T,\tau)$, from which it can be inferred that (Afsar et al. [15], Afsar [16]) $\Phi^*_{\lambda jk l}(\boldsymbol{y};\boldsymbol{k},\omega)$ depends on $\boldsymbol{k}_T$ only through its magnitude

$$k_T \equiv \sqrt{k_2^2 + k_3^2} \tag{20}$$

so that the generalized Reynolds stress spectral tensor

$$\Psi^*_{\lambda jkl}(\boldsymbol{y};\boldsymbol{k},\omega) \equiv \int_V e^{i\boldsymbol{k}\bullet\boldsymbol{\eta}}H_{\lambda jkl}(\boldsymbol{y},\boldsymbol{\eta},\omega)\,\mathrm{d}\boldsymbol{\eta} \tag{21}$$

will depend on $\nabla_{\boldsymbol{y}_T}S$ only through $|(\nabla_{\boldsymbol{y}_T}S)| = \sqrt{[1-M(\mathbf{y_T})\cos\theta]^2 c_\infty^2/\widetilde{c^2} - \cos^2\theta}$, which obviates the need to solve the Eikonal Eq. (19). It would again be impossible to define the Fourier transform in Eq. (21) [and, therefore, the spectral tensor (17)] if the autocovariance tensor (8) were replaced by the correlation tensor (11), since the latter quantity tends to a nonzero value as $\boldsymbol{\eta}\to\infty$.

IV. Modeling the Spectrum

Harper–Bourne [6] showed that the absolute value

$$R(\boldsymbol{y},\boldsymbol{\eta},\omega) \equiv |\tilde{R}(\boldsymbol{y},\boldsymbol{\eta},\omega)| \tag{22}$$

of the normalized fixed-frame spectrum [see Eq. (7)]

$$\tilde{R}(\boldsymbol{y},\boldsymbol{\eta},\omega) \equiv \frac{H_{1111}(\boldsymbol{y},\boldsymbol{\eta},\omega)}{H_{1111}(\boldsymbol{y},\mathbf{0},\omega)} \tag{23}$$

becomes frequency independent when the components of $\boldsymbol{\eta}$ are normalized by appropriate frequency-dependent length scales. But Goldstein and Leib [4] were able to make reasonably good jet noise predictions based on a nonseparable, moving-frame, space-time Reynolds stress autocovariance tensor of the form

$$R^M_{ijkl}(\hat{\xi}_1,\hat{\xi}_T,\hat{\tau}) = \hat{A}_{ijkl}\exp[-(\hat{\xi}_1^2+\beta^2+\hat{\tau}^2)^{1/2}+\hat{\gamma}] \tag{24}$$

where $\xi_i \equiv \eta_i - \delta_{1i}U_c\tau$, with $\beta^2 = \beta^2(\hat{\xi}_T)$ and $\hat{\gamma}^2 = \hat{\gamma}^2(\hat{\xi}_T)$ being arbitrary functions of $\hat{\xi}_T \equiv \sqrt{\hat{\xi}_2^2+\hat{\xi}_3^2}$ that vanish at $\hat{\xi}_T = 0$, $\hat{A}_{ijkl}$ is a parameter, and the variables $\hat{\xi}_i \equiv \xi_i/\hat{l}_i$ and $\hat{\tau} \equiv \tau\lambda$ are normalized by the characteristic length and time scales $\hat{l}_i$, $i = 1, 2, 3$, and $1/\lambda$, respectively. This functional form is consistent with the classical Taylor notion that the turbulence is nearly frozen and decays only slowly with time when measured in an appropriate moving reference frame. Figure 1 shows that it exhibits the usual space-time behavior observed for such functions as depicted, for example, in Fig. 2 taken from [6], which is similar to measurements obtained by other investigators (e.g., [7]). Tester and Morfey [26] discuss several other autocovariance models that have been proposed in the literature. However, unlike the Goldstein and Leib [4] result, none of these exhibit both the experimentally observed cusps at τ, $\boldsymbol{\eta}_T = 0$ as $\eta_1 \to 0$ and at $\boldsymbol{\eta} = 0$ as $\tau\to 0$. They also do not exhibit the increase in width with increasing streamwise separation distance shown in Fig. 2.

However, the fixed-frame autocovariance tensor

$$R_{ijkl} = A_{ijkl}e^{-X} \tag{25}$$

where

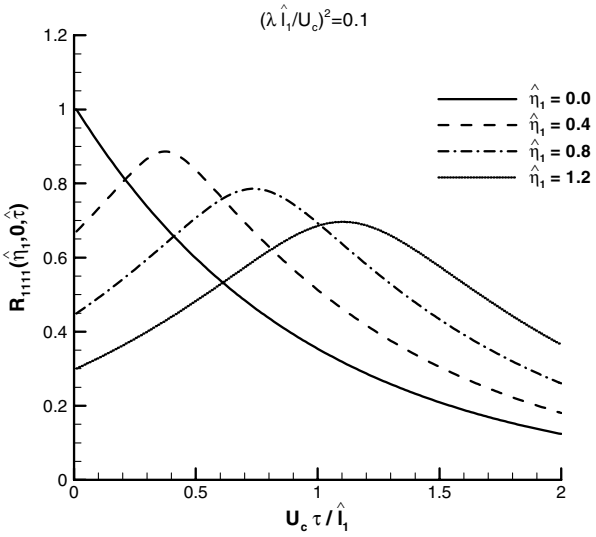

Fig. 1 Behavior of *moving-frame* autocovariance.

$$X(\tilde{\eta}_1,\tilde{\eta}_T,\tilde{\tau})=\sqrt{\tilde{\eta}_1^2+\tilde{\beta}^2+\tilde{\xi}_1^2} \tag{26}$$

$\xi_1 \equiv \eta_1 - U_c\tau$, with $\tilde{\beta}^2=\tilde{\beta}^2(\tilde{\eta}_T)$ an arbitrary function of $\tilde{\eta}_T \equiv \sqrt{\tilde{\eta}_2^2+\tilde{\eta}_3^2}$ that vanishes at $\tilde{\eta}_T=0$, A_{ijkl} is a parameter and the variables $\tilde{\xi}_1 \equiv \xi_1/l_0$, $\tilde{\eta}_i \equiv \eta_i/l_i$, $i=1,2,3$ are normalized by the intermediate length scales l_i, $i=0,1,2,3$, is also in qualitative agreement with the results in Fig. 2, as shown by Fig. 3. Since this result exhibits the experimentally observed cusps at τ, $\tilde{\boldsymbol{\eta}}_T=0$ as $\eta_1\to 0$ and at $\boldsymbol{\eta}=0$ as $\tau\to 0$, it is also consistent with all the usual experimental observations.

While the result in [4] might appear to be more in concert with the original Taylor hypothesis, Figs. 1–3 suggest that the present result is in somewhat better quantitative agreement with the Harper–Bourne measurements. Note that the normalized variables in Fig. 2 were obtained using the convection velocity and streamwise length scale given by Harper–Bourne. More important, it also yields a frequency-independent formula for $R(\boldsymbol{y},\boldsymbol{\eta},\omega)$ since the spectrum

$$H_{ijkl}(\boldsymbol{y},\boldsymbol{\eta},\omega)\equiv\frac{1}{2\pi}\int_{-\infty}^{\infty}e^{-i\omega\tau}R_{ijkl}(\boldsymbol{y},\boldsymbol{\eta},\tau)\,\mathrm{d}\tau = A_{ijkl}e^{-i\omega l_1\tilde{\eta}_1/U_c} \times\frac{2l_0[\tilde{\eta}_1^2(1+\tilde{\omega}^2)+\tilde{\beta}^2(1+\tilde{\omega}^2)]^{1/2}K_1([\tilde{\eta}_1^2(1+\tilde{\omega}^2)+\tilde{\beta}^2(1+\tilde{\omega}^2)]^{1/2})}{2\pi U_c(1+\tilde{\omega}^2)} \tag{27}$$

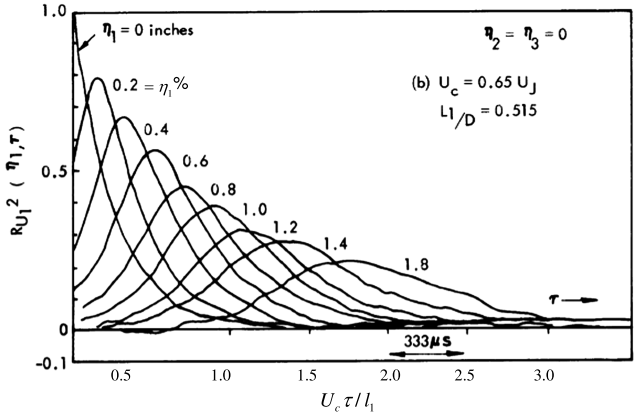

Fig. 2 Measurements of the autocovariance of the squares of the streamwise velocity fluctuations, $R_{U_1^2}(\boldsymbol{y},\boldsymbol{\eta},\tau)\equiv\lim_{T\to\infty}\frac{1}{2T}\int_{-T}^{T}[v_1'v_1'-\overline{v_1'v_1'}](\boldsymbol{y},\tau_0)[v_1'v_1'-\overline{v_1'v_1'}](\boldsymbol{y}+\boldsymbol{\eta},\tau_0+\tau)\,\mathrm{d}\tau_0$, from Harper–Bourne [6] (used with permission). Note that the generalized Reynolds stress autocovariance defined by Eq. (8) contains the instantaneous (mean plus fluctuating) density, whereas Harper-Bourne's [6] measurements do not.

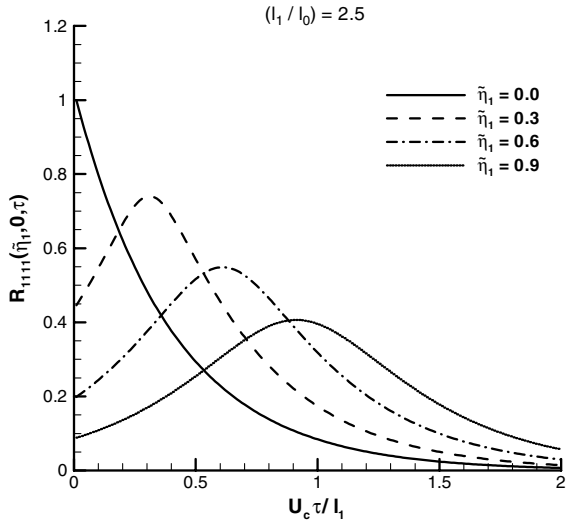

Fig. 3 Autocovariance function computed from Eq. (25).

where

$$\tilde{\omega}\equiv\omega l_0/U_c \tag{28}$$

and K_ν denotes the modified Bessel function of the second kind, can be rewritten as

$$H_{ijkl}(\boldsymbol{y},\boldsymbol{\eta},\omega)=A_{ijkl}e^{-i\omega l_1\tilde{\eta}_1/U_c}l_0\frac{(\tilde{\eta}_1^2+\bar{\beta}^2)^{1/2}K_1((\tilde{\eta}_1^2+\bar{\beta}^2)^{1/2})}{\pi U_c(1+\tilde{\omega}^2)} \tag{29}$$

with

$$\bar{\eta}_1^{\,2}\equiv\tilde{\eta}_1^2(1+\tilde{\omega}^2) \tag{30}$$

$$\bar{\eta}_i^{\,2}\equiv\eta_i^2/\bar{l}_i^{\,2}(\tilde{\omega}),\quad \text{for } i=1,2,3 \tag{31}$$

$$\bar{\beta}^{\,2}(\tilde{\eta}_T)\equiv(1+\tilde{\omega}^2)\tilde{\beta}^2(\tilde{\eta}_T) \tag{32}$$

$$\bar{\eta}_T^{\,2}\equiv\eta_2^2/\bar{l}_2^{\,2}(\tilde{\omega})+\eta_3^2/\bar{l}_3^{\,2}(\tilde{\omega}) \tag{33}$$

which implies that

$$\begin{gathered}\bar{l}_1\sim\tilde{\omega}^{-1},\qquad \bar{l}_2,\bar{l}_3\sim\tilde{\omega}^{-1/\alpha},\qquad 1\le\alpha<\infty,\quad \text{as }\tilde{\omega}\to\infty\\ \bar{l}_i=\mathcal{O}(1)\quad\text{as }\tilde{\omega}\to 0\end{gathered} \tag{34}$$

when $\bar{\beta}$ is set equal to $\bar{\eta}_T^{\alpha}$. Then, since

$$H_{ijkl}(\boldsymbol{y},\boldsymbol{0},\omega)=\frac{l_0A_{ijkl}}{\pi U_c(1+\tilde{\omega}^2)} \tag{35}$$

it follows that

$$\begin{aligned}\tilde{R}(\mathbf{y},\boldsymbol{\eta},\omega)&\equiv\frac{H_{1111}(\mathbf{y},\boldsymbol{\eta},\omega)}{H_{1111}(\mathbf{y},\mathbf{0},\omega)}\\ &=e^{-i\omega l_1\tilde{\eta}_1/U_c}(\bar{\eta}_1^2+\bar{\beta}^2)^{1/2}K_1((\bar{\eta}_1^2+\bar{\beta}^2)^{1/2})\end{aligned} \tag{36}$$

and, therefore, that $R(\boldsymbol{y},\boldsymbol{\eta},\omega)=R(\boldsymbol{y},\overline{\boldsymbol{\eta}})$ when $\bar{\beta}$ is set equal to $\bar{\eta}_T^{\alpha}$, i.e., that $R(\boldsymbol{y},\boldsymbol{\eta},\omega)$ will be frequency independent when expressed in terms of the normalized $\bar{\boldsymbol{\eta}}$ variables, which shows that the present model is consistent with Harper–Bourne's [6] rather surprising observation.

The fixed-frame spectral tensor (21), which is related to the spectral tensor $\Phi^*_{\lambda jkl}(\boldsymbol{y};\boldsymbol{k},\omega)$ that appears in Eq. (16) by [see Eqs. (9), (17), and (21)] by

$$\Phi^*_{vj\mu l} = \varepsilon_{vj,\sigma m}\Psi^*_{\sigma m\lambda n}\varepsilon_{\mu l,\lambda n} \tag{37}$$

can be written in terms of the scaled frequency-dependent wave numbers $\bar{\boldsymbol{k}}_T \equiv \{k_2\bar{l}_2, k_3\bar{l}_3\}$, $\bar{k}_T \equiv |\bar{\boldsymbol{k}}_T|$ and

$$\bar{k}_1 \equiv (k_1 - \omega/U_c)\bar{l}_1 \tag{38}$$

as

$$\Psi^*_{ijkl}(k_1, \boldsymbol{k}_T, \omega) = -\frac{2\pi l_0 \bar{l}_1 \bar{l}_2 \bar{l}_3 A_{ijkl}}{U_c(1+\tilde{\omega}^2)}\frac{1}{\bar{k}_1}\frac{\partial}{\partial \bar{k}_1}G_0(\bar{\boldsymbol{k}}_T, \bar{k}_1, \tilde{\omega}) \tag{39}$$

where

$$\begin{aligned} G_0(\bar{\boldsymbol{k}}_T, \bar{k}_1, \tilde{\omega}) &\equiv \frac{1}{2\pi(1+\bar{k}_1^2)^{1/2}}\int e^{i\bar{\boldsymbol{\eta}}_T\bullet\bar{\boldsymbol{k}}_T - \bar{\beta}(\bar{\eta}_T)(1+\bar{k}_1^2)^{1/2}}\,\mathrm{d}\bar{\boldsymbol{\eta}}_T \\ &= \frac{1}{(1+\bar{k}_1^2)^{1/2}}\int_0^\infty J_0(\bar{\eta}_T\bar{k}_T)e^{-\bar{\beta}(\bar{\eta}_T)\sqrt{1+\bar{k}_1^2}}\bar{\eta}_T\,\mathrm{d}\bar{\eta}_T \end{aligned} \tag{40}$$

is just the Hankel transform of $(1+\bar{k}_1^2)^{-1/2}\exp[-\bar{\beta}\sqrt{1+\bar{k}_1^2}]$.

Since Harper–Bourne [6] was best able to fit his data with

$$R(\boldsymbol{y}, \boldsymbol{\eta}, \omega) = e^{-\sqrt{\bar{\eta}_1^2 + \bar{\eta}_T^4}} \tag{41}$$

it is appropriate to set $\bar{\beta}$ equal to $\bar{\eta}_T^2$. Figure 4 shows the functional form (36) compared with the Harper–Bourne [6] fit. The scaled transverse length scales $\bar{l}_{2,3}$ and the Hankel transform G_0 will then be given by ([27])

$$\bar{l}_{2,3} = l_{2,3}/(1+\tilde{\omega}^2)^{1/4} \tag{42}$$

and

$$G_0(\bar{k}_T, \bar{k}_1, \tilde{\omega}) = \frac{1}{2(1+\bar{k}_1^2)}e^{-\bar{k}_T^2/4(1+\bar{k}_1^2)^{1/2}} \tag{43}$$

respectively, which implies that the spectral tensor $\Psi^*_{\lambda jkl}(\boldsymbol{y}; \boldsymbol{k}, \omega)$ will depend on the transverse component $\boldsymbol{k}_T$ of $\boldsymbol{k}$ only through

$$\bar{k}_T^2 \equiv (\bar{l}_2 k_2)^2 + (\bar{l}_3 k_3)^2 \tag{44}$$

But since the results in [4] are based on the assumption that R_{ijkl} depends on the transverse component of the separation vector only through its magnitude, and since [14] shows that this assumption is in good agreement with LES data (see discussion in Sec. I), we suppose that

$$\bar{k}_T^2 \equiv k_2^2\bar{l}_2^2 + k_3^2\bar{l}_3^2 = (\bar{l}_T k_T)^2 \tag{45}$$

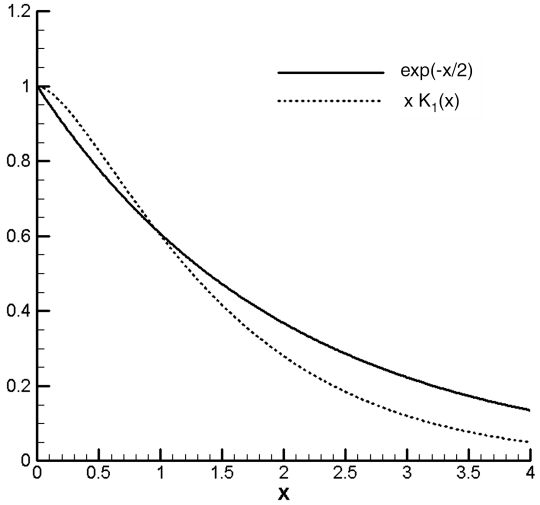

Fig. 4 Comparison of the function in Eq. (36) with the exponential Eq. (41).

where k_T^2 is obtained using the right side of Eq. (19), and

$$\bar{l}_T \equiv \sqrt{\bar{l}_2^2 + \bar{l}_3^2} \tag{46}$$

Equation (25) can be generalized to account for the experimentally observed long-range oscillations in the autocovariance function by putting

$$R_{ijkl} = \sum_{m=0}^{\infty}\sum_{l=0}^{\infty} a_{m,l}D_1^m D_\tau^l e^{-X} \tag{47}$$

where the $a_{m,l}$ are parameters and the operators D_κ^n, for $\kappa = \tau, 1$ are defined by

$$\begin{aligned} D_1 &\equiv \left[\tilde{\eta}_1 + \left(\frac{l_1}{l_0}\right)\tilde{\xi}_1\right]\left[\frac{\partial}{\partial\tilde{\eta}_1} + \left(\frac{l_1}{l_0}\right)\frac{\partial}{\partial\tilde{\xi}_1}\right], \qquad D_\tau \equiv \tilde{\xi}_1\frac{\partial}{\partial\tilde{\xi}_1}, \\ D_\kappa^0 &\equiv 1, \qquad D_\kappa^n \equiv D_\kappa \ldots D_\kappa, \qquad n \text{ times} \end{aligned} \tag{48}$$

Then, since Eqs. (39) and (43) can also be written as

$$\begin{aligned} &\Psi^*_{ijkl}(k_1, \boldsymbol{k}_T, \omega) \\ &\quad = -\frac{\pi l_0 l_1 \bar{l}_T^2(1+\tilde{\omega}^2)^{1/2}A_{ijkl}}{U_c}\frac{1}{R}\frac{\partial}{\partial R}\frac{1}{(1+R^2)}e^{-\bar{k}_T^2/4(1+R^2)^{1/2}} \end{aligned} \tag{49}$$

for $l_2 = l_3 = l_T$, where

$$R^2 \equiv \tilde{\omega}^2 + \tilde{k}_1^2 \tag{50}$$

$$\tilde{k}_1 \equiv (k_1 - \omega/U_c)l_1 \tag{51}$$

and

$$\tilde{k}_T^2 \equiv (k_2^2 + k_3^2)\bar{l}_T^2(1+\tilde{\omega}^2)^{1/2} \tag{52}$$

this implies that

$$\begin{aligned} \Psi^*_{ijkl}(k_1, \boldsymbol{k}_T, \omega) &= -\frac{\pi l_0 l_1 \bar{l}_T^2(1+\tilde{\omega}^2)^{1/2}A_{ijkl}}{U_c} \\ &\quad \times \sum_{m,l=0}^{\infty} a_{m,l}(-1)^{m+l}D_{k_1}^m D_\omega^l \frac{1}{R}\frac{\partial}{\partial R}\frac{1}{(1+R^2)}e^{-\bar{k}_T^2/4(1+R^2)^{1/2}} \end{aligned} \tag{53}$$

where $D_{k_1} \equiv \left(\frac{l_1}{l_0}\frac{\partial}{\partial\tilde{\omega}} + \frac{\partial}{\partial\tilde{k}_1}\right)\left(\frac{l_1}{l_0}\tilde{\omega} + \tilde{k}_1\right)$, $D_\omega \equiv \frac{\partial}{\partial\tilde{\omega}}\tilde{\omega}$, $\partial/\partial\tilde{\omega}$ is at constant $\tilde{k}_1$ and vice versa.

Retaining the first few $a_{n,0}$ terms in Eq. (47) yields

$$\begin{aligned} R_{ijkl} = \Bigg\{ &a_{0,0} - Z(a_{1,0} + 2a_{2,0}\tilde{l}^2 + 4a_{3,0}\tilde{l}^4) + Z^2\left(1+\frac{1}{X}\right)(a_{2,0} \\ &+ 6a_{3,0}\tilde{l}^2) - Z^3\left[1 + \frac{3}{X}\left(1+\frac{1}{X}\right)\right]a_{3,0}\Bigg\}e^{-X} \end{aligned} \tag{54}$$

where

$$\tilde{l}^2 \equiv (l_1^2 + l_0^2)/l_0^2 \tag{55}$$

and

$$Z \equiv \frac{1}{X}\left(\tilde{\eta}_1 + \frac{l_1}{l_0}\tilde{\xi}_1\right)^2 \tag{56}$$

The corresponding two- and three-term expressions for the spectral tensor components (53) are written out in the Appendix.

Equations (30), (31), and (42) imply that the formulas for the frequency-dependent length scales will be different from those proposed by Harper–Bourne [6], with the most significant discrepancy being that the asymptotic behavior [Eq. (34)] of the transverse length scales does not match those proposed by Harper–Bourne [6] (see also Morris and Zaman [7,8]). However, the Harper–Bourne [6] result suggests that it may be better to base this modeling

on the spectral tensor (29–33) rather than on the original space-time form (25) and (26), since the former can be generalized by introducing different formulas for the frequency-dependent length scales $\bar{l}_i$. In particular, the high-frequency roll-off of the transverse length scales can be made to match the Harper–Bourne [6] result, when $\bar{\beta}$ is equal to $\bar{\eta}_T^2$, by replacing the original frequency scaling Eq. (42) by

$$\bar{l}_{2,3} = \frac{l_{2,3}}{[1+\tilde{\omega}^2(1+b\tilde{\omega}^2)/(1+b)]^{1/4}} = \bar{l}_T/\sqrt{2} \tag{57}$$

where b is a (relatively small) constant. This modification only changes the transverse length scales and, therefore, does not change the shape of the streamwise autocovariance function shown in Fig. 3. The more general, Harper–Bourne-type, frequency-dependent length scales can also be exploited (i.e., modified) to better capture the large-scale structures, which are believed to be the dominant source of the small-angle radiation at high Mach numbers, by starting from the autocovariance spectrum Eqs. (29–33) (with appropriate models for the frequency-dependent transverse length scales $\bar{l}_2$, $\bar{l}_3$) instead of from the autocovariance Eqs. (25) and (26). But this is equivalent to starting with the spectral tensor (39) and (40), with an appropriate model for the frequency-dependent transverse length scale $\bar{l}_T$ or, more generally, starting from the spectral Eq. (53) (with an appropriate model for $\bar{l}_T$) instead of from the autocovariance, Eq. (47). Previous attempts to use frequency-dependent length scale models of the Fourier-transformed autocovariance tensor can be found in [28–30]. Since the models for the time and streamwise spatial separation scales enter through the space-time covariance Eqs. (25) and (26), while the transverse separation dependence is specified in terms of the transverse frequency-dependent length scale $\bar{l}_T$ that enters through the spectral form (53), the present approach can be thought of as a hybrid between time-domain and frequency-domain modeling.

Although the frequency-dependent length scale model (57) matches the high-frequency roll-off of the Harper–Bourne [6] form, it leads to a nonintegrable form for the acoustic spectrum. To see this, note that Eqs. (16), (19), (39), (43), and (45) imply that

$$\bar{k}_T^2 \approx (\omega\bar{l}_T/c_\infty)^2\{[1-M(\boldsymbol{y}_T)\cos\theta]^2 c_\infty^2/\widetilde{c^2} - \cos^2\theta\} \quad \text{as } \omega\to\infty \tag{58}$$

remains finite as $\omega\to\infty$ and vanishes when $[1-M(\boldsymbol{y}_T)\cos\theta]^2 c_\infty^2/\widetilde{c^2} \to \cos^2\theta$, and that

$$\Psi^*_{ijkl}(k_1,\boldsymbol{k}_T,\omega) \to \frac{\pi l_0 \bar{l}_1 \bar{l}_T^2 A_{ijkl}}{U_c\tilde{\omega}^2} \times \exp-\left[\frac{(\omega\bar{l}_T/c_\infty)^2}{4\sqrt{1+\tilde{k}_1^2}}\{[1-M(\boldsymbol{y}_T)\cos\theta]^2 c_\infty^2/\widetilde{c^2} - \cos^2\theta\}\right] \quad \text{as } \omega\to\infty \tag{59}$$

so

$$\Psi^*_{ijkl}(k_1,\boldsymbol{k}_T,\omega) \propto \omega^{-5} \quad \text{as } \omega\to\infty \tag{60}$$

when the frequency-dependent length scales are given by Eq. (57), which implies that the corresponding far-field acoustic spectrum decays like $1/\omega$ and is, therefore, nonintegrable (see also [4]). But since it would be hard to tell whether $\bar{l}_{2,3}$ decayed like $\omega^{-5/4}$ instead of like ω^{-1} from the Harper–Bourne [6] or the Morris and Zaman [7,8] data, it is reasonable to obtain an integrable spectrum by putting

$$\bar{l}_{2,3} = \frac{l_{2,3}}{[1+\tilde{\omega}^2(1+b\tilde{\omega}^3)/(1+b)]^{1/4}} = \bar{l}_T/\sqrt{2} \tag{61}$$

Changing the frequency-dependent length scale $\bar{l}_T$ in Eqs. (52) and (53) is equivalent to changing it in the normalized spectrum $H_{ijkl}(\boldsymbol{y},\boldsymbol{\eta},\omega)/H_{ijkl}(\boldsymbol{y},\boldsymbol{0},\omega)$ of Eq. (36). So the former results can, for example, be made more consistent with the Harper–Bourne result by using Eq. (57) [or Eq. (61)] for $\bar{l}_2 = \bar{l}_3 = \bar{l}_T/\sqrt{2}$. Figure 5 is a plot of the transverse frequency-dependent length scale model (61), along with the functional form used by Harper–Bourne [6] to fit his results for the spatial decay scales obtained from his coherence measurements. The models are quite similar and, as mentioned above, it is difficult to distinguish their slightly different high-frequency asymptotic behaviors.

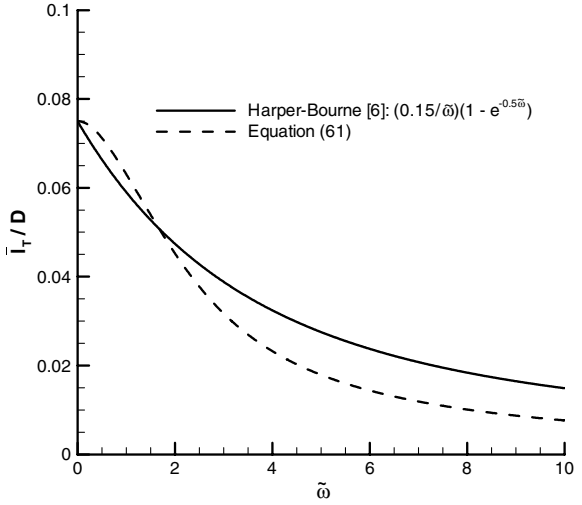

Fig. 5 Comparison of the transverse frequency-dependent length scale model Eq. (61) with Harper–Bourne's [6] formula.

As noted above, this modification does not change the shape of the streamwise autocovariance function shown in Fig. 3, which means that the spectrum Eq. (36) is still in good qualitative agreement with the usual experimental data. Equations (10) and (37) can be used to calculate the spectral function $\Phi^*_{\lambda jkl}(\boldsymbol{y};\boldsymbol{k},\omega)$ that appears in Eq. (16).

V. Results and Discussion

The acoustic predictions require information about the various components of the turbulence autocovariance amplitudes $R_{ijkl}(\boldsymbol{y},\boldsymbol{0},0)$. Goldstein and Leib [4] and Karabasov et al. [23,24] assume that

$$R_{ijkl}(\boldsymbol{y},\boldsymbol{0},0) \approx C_{ijkl}(\bar{\rho}k)^2 \tag{62}$$

where the C_{ijkl} are constants and k now denotes the turbulent kinetic energy determined from a RANS computation. Goldstein and Leib [4] use the quasi-normal and axisymmetry assumptions, along with experimental data, to determine the C_{ijkl}, whereas Karabasov et al. [20,21] use information from a LES to determine these quantities. The specific values used in [4] were: $C_{1111} = 1.28$; $C_{2222} = C_{3333} = C_{2233} = 0.72$; $C_{1122} = C_{1133} = C_{1212} = 0.96$, but it was incorrectly stated in that reference that $C_{1122} = C_{1212}$ by definition. Also, the equations defining the C_{ijkl}, beginning on the ninth line of p. 322, should read: $C_{1111} = 2(\overline{v_1'^2})^2/k^2$, etc.

The computations in this paper are based on Eqs. (A4) and (62) with the $a_{n,0}/a_{0,0}$ taken to be independent of the source location $\boldsymbol{y}$, and $b = 0.1$ for the quadrupolelike terms and $b = 0.5$ in the dipolelike term, as identified in [4]. The former approximation is introduced because of the lack of detailed information about the variation of the turbulence spectrum within the jet, and may not provide a very good representation of the real turbulent autocovariance functions in certain regions of the flow. The specific values used for the ratios, $a_{n,0}/a_{0,0}$, of the coefficients in the truncated series representation Eq. (A4) are indicated in Table 1.

Recently obtained experimental data [7–14] and LES results [31] are used to scale the turbulent Reynolds stress autocovariance amplitudes, relative to the purely axial component. The turbulence is assumed to be statistically axisymmetric, but not quasi normal

Table 1 Coefficients in the truncated series representation of the turbulence spectrum

Component	$a_{1,0}/a_{0,0}$	$a_{2,0}/a_{0,0}$	$a_{3,0}/a_{0,0}$
1111	0.073	0.070	-8.48×10^{-4}
2222 = 3333	0.519	0.049	−0.0097
1122 = 1133	0.103	0.079	0.0
1212	0.559	−0.006	−0.015

Table 2 Constants used to determine the length scales for the indicated components of the turbulence auto- covariance

Component	C_0	C_1	C_T
1111	0.7	1.2	0.4
2222 = 3333	0.7	0.8	0.89
1122 = 1133	0.7	1.1	1.0
1212	1.05	1.0	1.1

as assumed in [4]. Specifically, we set $C_{2222} = C_{3333} = 0.159C_{1111}$, $C_{2233} = 0.0$, $C_{1122} = C_{1133} = 0.047C_{1111}$, and $C_{1212} = 0.228C_{1111}$. The absolute level of the turbulence (and therefore of the sound) is set by putting $C_{1111} = 2(\overline{v_1'^2})^2/k^2$ where $\boldsymbol{v}' = \{v_1', v_2', v_3'\}$ and $\overline{v_1'^2} = 0.8k$, as suggested by flow measurements in the jets considered in this paper. The length scales, l_1, $l_2 = l_3 = l_T$, are related to the RANS computations by setting $l_0 = C_0 k^{3/2}/\varepsilon$, $l_1 = C_1 k^{3/2}/\varepsilon$ and $l_T = C_T k^{3/2}/\varepsilon$. The specific values used for the constants in these length scales are shown in Table 2.

As in [4], we set $U_c = 0.68U_{cl}$, where U_{cl} is the jet centerline velocity, for the quadrupolelike source terms, but, to better represent the large-scale turbulent structures in the jet, we use $U_c = 0.8U_{cl}$ in the dipolelike term. All of the supersonic calculations in this paper are based on the composite Green's function solution of [4] that accounts for both actual and detuned critical layers.

Figure 6 shows comparisons of the resulting predictions with the SHJAR data. Predictions have been made for three unheated jet flow conditions, corresponding to jet exit acoustic Mach numbers of 0.5, 0.9, and 1.4. Each plot shows results for the far-field acoustic spectra corresponding to a fixed far-field observer polar angle (measured from the downstream jet axis) at the three jet Mach numbers considered. Seven polar angles are shown, covering the range of interest. The predictions, which are, of necessity, based on a number of questionable assumptions about the turbulence (such as the assumed constancy of the $a_{n,0}$), are generally within about 2 dB of the

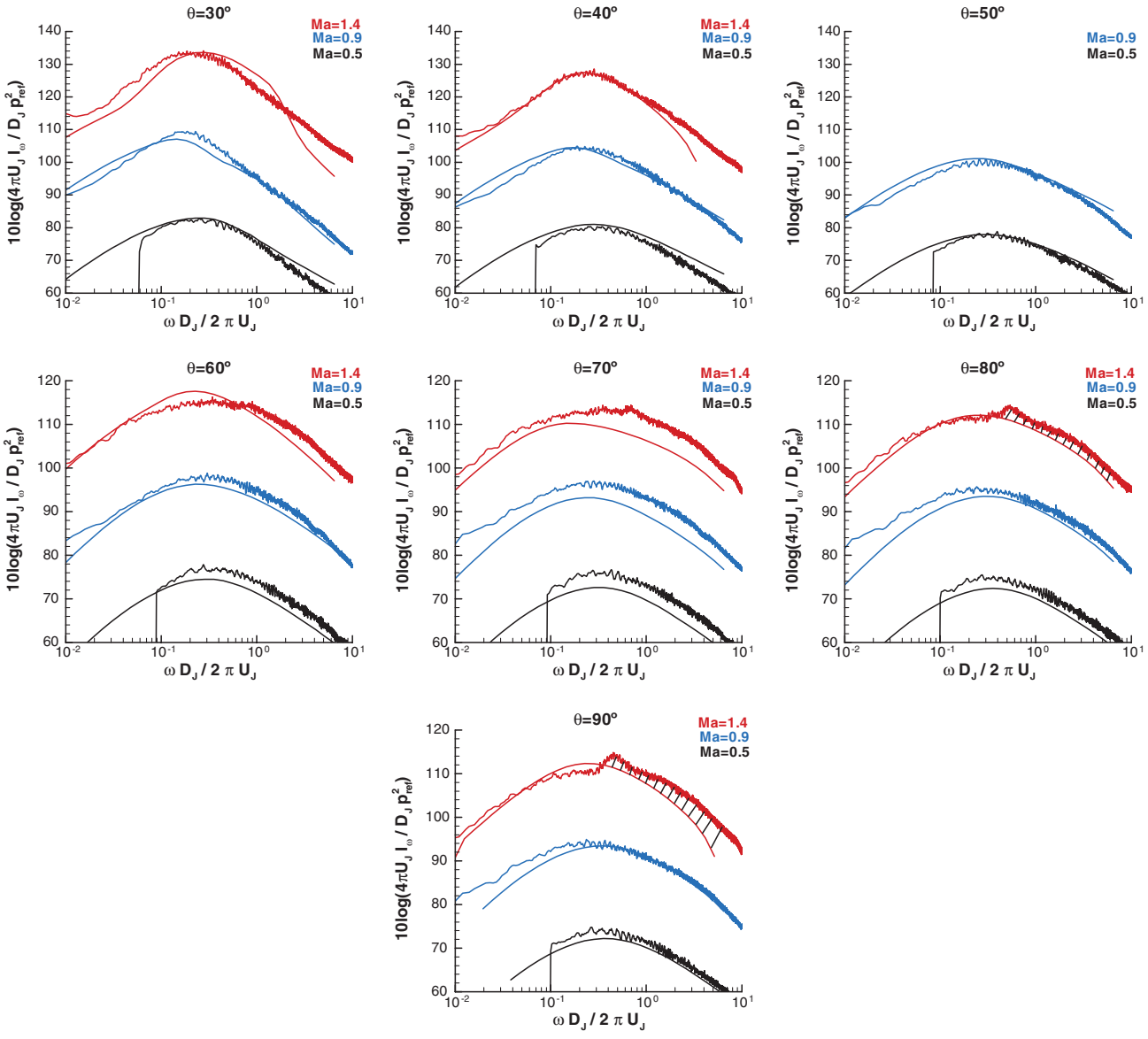

Fig. 6 Comparisons of predictions based on equation 6.27 of Goldstein and Leib [4] and the present hybrid source model with the SHJAR acoustic data.

data. Figure 28 of [32] suggests that the range of variation of data taken for the same nominal flow conditions in different facilities can also be about 2 dB, although the uncertainty in the SHJAR data has been documented as closer to 1 dB [33]. The accuracy of the noise predictions is also limited by the inherent uncertainty in the RANS solution. The model is able to capture the large increase in sound at supersonic speeds for angles near the jet axis. The hatched regions in the plots for $\theta = 80$ and 90° in Fig. 6 indicate where the data are believed to be dominated by shock-associated noise, caused by slight differences in the actual exit pressure from its perfectly expanded value. The present model only accounts for the turbulent mixing noise, and not the shock-associated noise. Morris and Miller [34] recently developed a prediction scheme for the broadband component of this noise in imperfectly expanded supersonic jets using an (different) acoustic analogy. There is a critical layer, at the transverse location where $1 - M(y_t)\cos\theta = 0$, for angles $\theta \leq 45^\circ$ in the $M_a = 1.4$ supersonic case shown in Fig. 6. But the sound field may also be affected by another detuned critical layer with even more complicated asymptotic structure, at angles that are a little larger than that. We, therefore, do not show any results for $\theta = 50^\circ$ and $M_a = 1.4$ in this figure.

Figure 7 shows the contributions to the total acoustic spectrum from the individual terms in the equation 6.27 of [4]. The results lend further support to the idea of a two-source model for jet noise discussed in [4] and in greater detail in [16] (see also references therein). The results in Fig. 7 show that the far-field acoustic spectrum is dominated by the contribution from quadrupolelike terms (i.e., terms that behave like ω^4 as $\omega \to 0$) at subsonic Mach numbers, and at 90 degrees to the jet axis at transonic and supersonic Mach numbers, whereas the dipolelike term (which behaves like ω^2 as $\omega \to 0$) is the dominant term for supersonic speeds at small angles to the jet axis. The present paper suggests that the strong directionality of the latter term is now almost entirely due to mean flow interaction effects and retarded time variations across the source region. The acoustic spectra of transonic and supersonic jets at intermediate angles contain contributions from both types of terms.

Figure 8 shows the contributions to the acoustic spectra from various axial slices through the jet for different polar angles and Mach numbers. The relevant potential core lengths, determined from mean flow measurements [11,12], are indicated in the captions. At small angles to the downstream jet axis, particularly at the higher Mach numbers, the overall spectral peak is not too far above the peaks from the slice contributions from near the end of the potential core, which tend to be considerably higher than the peaks of the slice contributions from the remainder of the jet. At the sideline angles (particularly 90 degrees), the peak in total spectrum is considerably higher than the peaks from the individual slice contributions and the peak levels of the latter are nearly equal for a larger number of slices. This suggests that sound radiated to the peak noise direction (around 30 degrees to the jet axis) is primarily generated near, and just downstream of, the end of the potential core, whereas that radiated to the sideline directions is generated over a broader range of source locations in the jet.

The results presented in this paper (as well as those in [4]) suggest that relatively subtle characteristics of the Reynolds stress autocovariance function model can have a large effect on the predictions

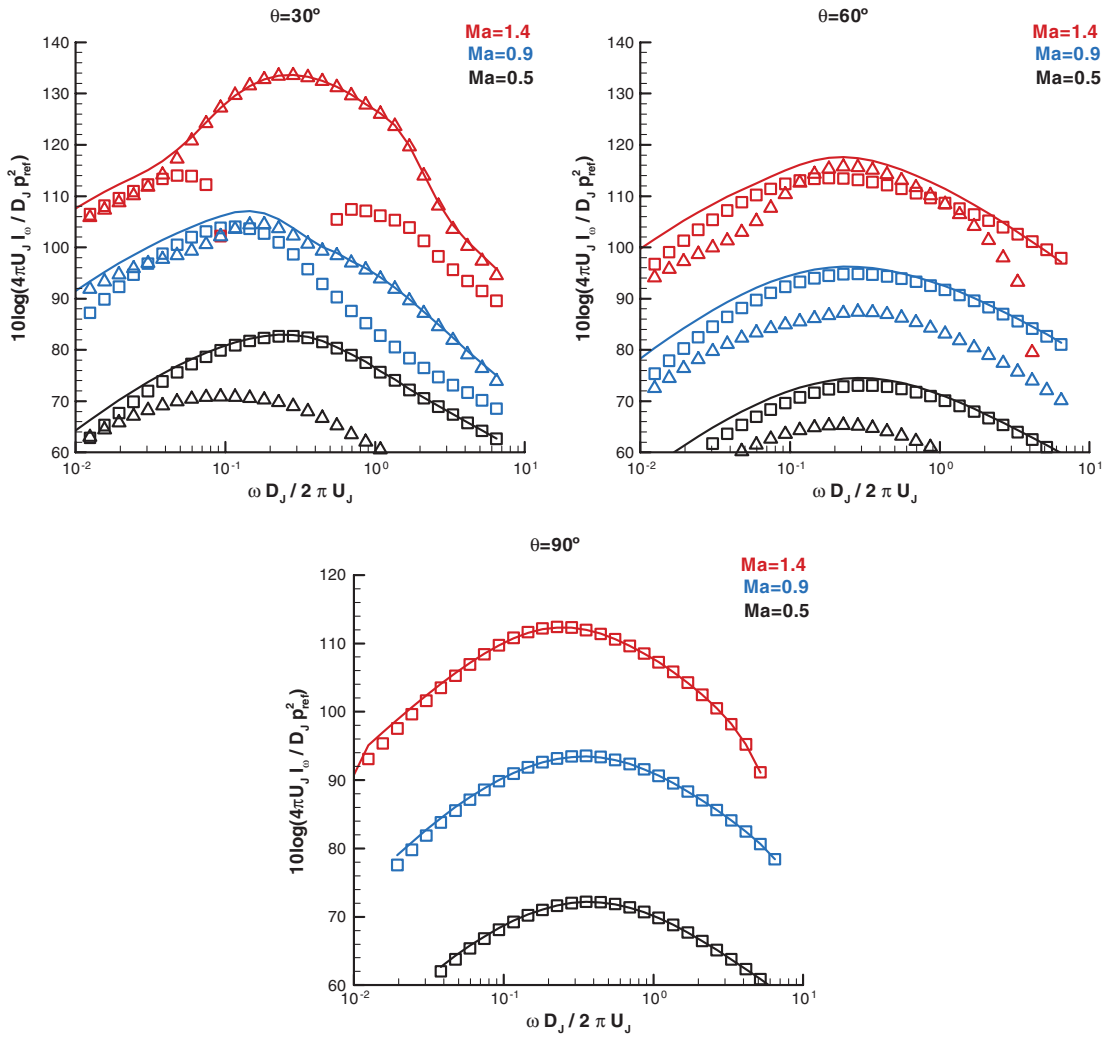

Fig. 7 Contributions to the predicted acoustic spectra from individual components. Solid curves, total spectrum; squares, quadrupolelike term, and triangles, dipolelike term.

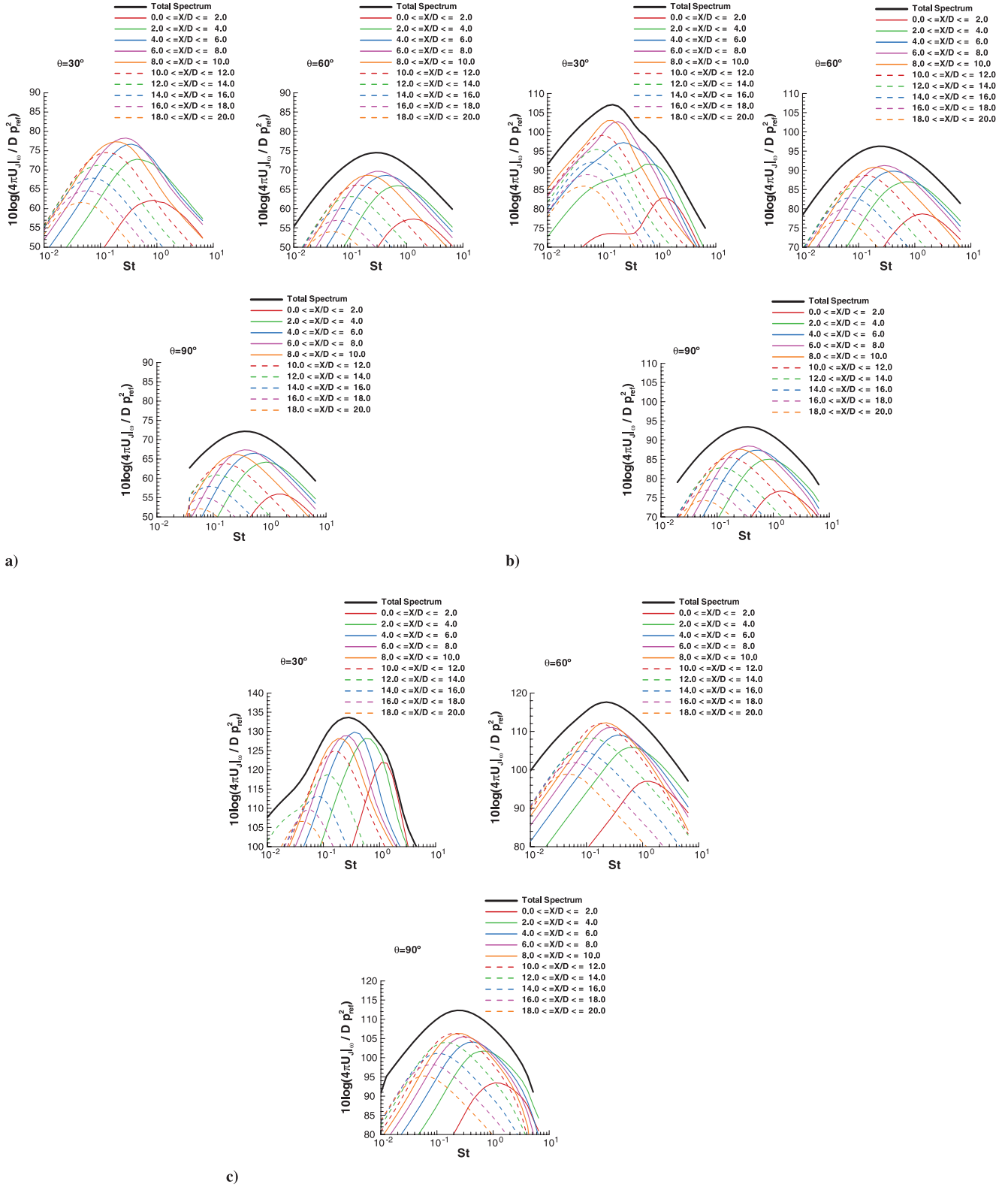

Fig. 8 Contributions to the predicted spectra from various axial slices through the jet: a) $Ma = 0.5$, end of the potential core at $x_c/D = 5.0$; b) $Ma = 0.9$, end of the potential core at $x_c/D = 6.5$; and c) $Ma = 1.4$, end of the potential core at $x_c/D = 8.0$.

for the acoustic radiation, particularly at high Mach number and shallow angles to the jet axis. Figure 9 shows the independent components of the Reynolds stress autocovariance tensor, which appear in the formula for the acoustic spectrum for values of the ratios $a_{n,0}/a_{0,0}$ given in Table 2 (i.e., those used in the noise predictions) as functions of the normalized variables defined in Sec. IV. The autocovariance R_{1111} of the (density-weighted) streamwise velocity squares, which appears in the quadrupolelike term, has a well defined cusp at $\tau = 0$ when $\eta_1 = 0$, and closely resembles the experimental results shown in Fig. 2, as well as those of other investigators (e.g., [7]). It tends to remain positive for most values η_1 and τ, which is consistent with the arguments given in [7] based on the quasi normal hypothesis, although we do not use this hypothesis here. The R_{1122} covariance, which also appears in the quadrupolelike term, is very

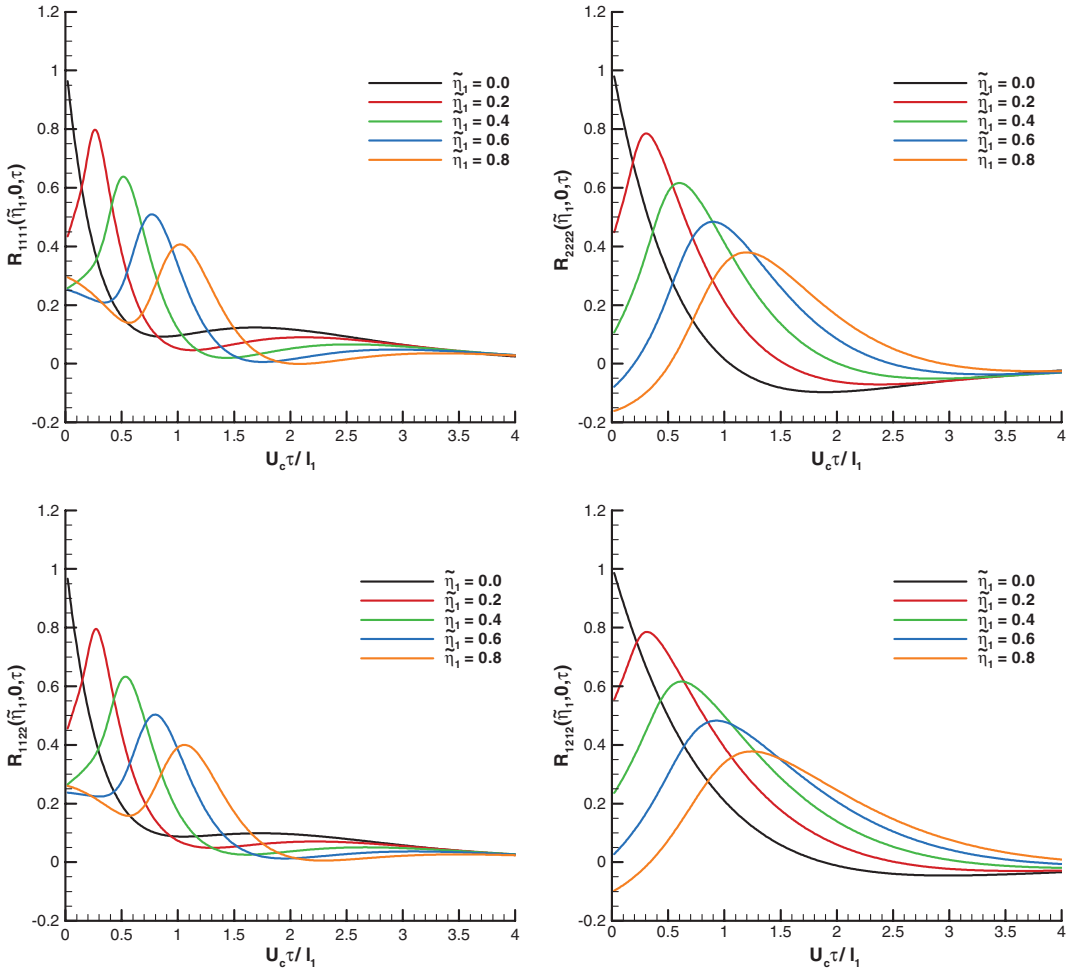

Fig. 9 Shapes of the Reynolds stress autocovariance components for the model coefficients used in the predictions.

similar. Our model for the autocovariance R_{2222} and, to a lesser extent, the shear stress autocovariance, R_{1212}, which appears in the dipolelike term, have regions of negative correlation.

VI. Conclusions

The acoustic analogy formulation of [5] relates the far-field acoustic spectrum to the product of a propagator and the space-time Fourier transform of the fluctuating Reynolds stress autocovariance tensor. The present paper introduces a new fixed-frame model for this tensor, which is more consistent with characteristics observed in recent experimental measurements of turbulence in jets than the moving-frame model used in [4]. This significantly diminishes source convection effects and the predicted directionality of the radiated sound can, therefore, be attributed to mean flow interaction effects and retarded time variations across the source region.

The result is used to predict the radiated sound field from three unheated jets, with jet exit acoustic Mach numbers of 0.5, 0.9, and 1.4, and comparisons are made with data taken in the SHJAR at NASA John H. Glenn Research Center at Lewis Field. The predictions of [4] were in reasonably good agreement with this data at observation angles of 30 and 90 deg, but were found to be in error at intermediate angles. The predictions based on the present model are shown to be in much better agreement with the data at these angles. The new model contains a number of "parameters" that are expected to vary with source location, but were treated as constants because of the lack of detailed information about the variation of the turbulence spectrum within the jet. Efforts are currently under way to obtain this information and the data will be used to properly account for the variation in these parameters when it becomes available. The hope is that the improved model will produce more reliable predictions outside the range of flow conditions for which they have been calibrated.

Appendix: Higher-Order Terms in the Reynolds Stress Autocovariance Formula

Equation (53) becomes

$$\Psi^*_{ijkl}(k_1,\boldsymbol{k}_T,\omega) = -\frac{\pi l_0 l_1 \bar{l}_T^2 (1+\tilde{\omega}^2)^{1/2} A_{ijkl}}{2U_c}\left\{a_{00} - a_{10}\left(\frac{l_1}{l_0}\frac{\partial}{\partial\tilde{\omega}} + \frac{\partial}{\partial\tilde{k}_1}\right)\left(\frac{l_1}{l_0}\tilde{\omega}+\tilde{k}_1\right) + a_{20}\left[\left(\frac{l_1}{l_0}\frac{\partial}{\partial\tilde{\omega}} + \frac{\partial}{\partial\tilde{k}_1}\right) \times \left(\frac{l_1}{l_0}\tilde{\omega}+\tilde{k}_1\right)\right]^2\right\}\frac{1}{R}\frac{\partial}{\partial R}\frac{1}{(1+R^2)}e^{-\tilde{k}_T^2/4(1+R^2)^{1/2}} \tag{A1}$$

when the series (47) is truncated after the second term. Or since

$$\left(\frac{l_1}{l_0}\frac{\partial}{\partial\tilde{\omega}} + \frac{\partial}{\partial\tilde{k}_1}\right)\left(\frac{l_1}{l_0}\tilde{\omega}+\tilde{k}_1\right) = \left(\frac{l_1}{l_0}\right)^2 + 1 + \left(\frac{l_1}{l_0}\tilde{\omega}+\tilde{k}_1\right)\left(\frac{l_1}{l_0}\frac{\partial}{\partial\tilde{\omega}} + \frac{\partial}{\partial\tilde{k}_1}\right) = \left(\frac{l_1}{l_0}\right)^2 + 1 + \frac{(k_1 l_1)^2}{R}\frac{\partial}{\partial R} + \left[\left(\frac{l_1}{l_0}\right)^2 + 1\right]k_1\left(\frac{\partial}{\partial k_1}\right)_R \tag{A2}$$

this can be written as

$$\Psi^*_{ijkl}(k_1,\boldsymbol{k}_T,\omega) = -\frac{\pi l_0 l_1 \bar{l}_T^2 A_{ijkl}(1+\tilde{\omega}^2)^{1/2}}{2U_c}\left\{a_{00} - a_{10}\tilde{l}^2 - a_{10}\frac{(k_1 l_1)^2}{R}\frac{\partial}{\partial R} + a_{20}\left[\left[\tilde{l}^2 + \frac{(k_1 l_1)^2}{R}\frac{\partial}{\partial R}\right]^2 + \frac{2(k_1 l_1)^2}{R}\tilde{l}^2\frac{\partial}{\partial R}\right]\right\}\frac{1}{R}\frac{\partial}{\partial R}\frac{1}{(1+R^2)}e^{-\tilde{k}_T^2(1+\tilde{\omega}^2)^{1/2}/4(1+R^2)^{1/2}}$$

$$= -\frac{\pi l_0 l_1 \bar{l}_T^2 A_{ijkl}(1+\tilde{\omega}^2)^{1/2}}{2U_c}\left[a_{00} - a_{10}\tilde{l}^2 + a_{20}\tilde{l}^4 + (4a_{20}\tilde{l}^2 - a_{10})(k_1 l_1)^2\left(\frac{1}{R}\frac{\partial}{\partial R}\right) + a_{20}(k_1 l_1)^4\left(\frac{1}{R}\frac{\partial}{\partial R}\right)^2\right]\frac{1}{R}\frac{\partial}{\partial R}\frac{1}{(1+R^2)}e^{-\tilde{k}_T^2(1+\tilde{\omega}^2)^{1/2}/4(1+R^2)^{1/2}} \quad \text{(A3)}$$

where $\bar{k}_T$ and $\tilde{l}^2$ are defined by Eqs. (45) and (55), respectively, and the $\partial/\partial R$ derivative is carried out at constant $\tilde{\omega}$ and $\bar{k}_T$. Similarly at the next order

$$\Psi^*_{ijkl}(k_1,\boldsymbol{k}_T,\omega) = -\frac{\pi l_0 l_1 \bar{l}_T^2 A_{ijkl}(1+\tilde{\omega}^2)^{1/2}}{2U_c}\left[a_{00} - a_{10}\tilde{l}^2 + a_{20}\tilde{l}^4 - a_{30}\tilde{l}^6 - (13a_{30}\tilde{l}^4 - 4a_{20}\tilde{l}^2 + a_{10})(k_1 l_1)^2\left(\frac{1}{R}\frac{\partial}{\partial R}\right) + (a_{20} - 9a_{30}\tilde{l}^2)(k_1 l_1)^4\left(\frac{1}{R}\frac{\partial}{\partial R}\right)^2 - a_{30}(k_1 l_1)^6\left(\frac{1}{R}\frac{\partial}{\partial R}\right)^3\right]\frac{1}{R}\frac{\partial}{\partial R}\frac{1}{(1+R^2)}e^{-\tilde{k}_T^2(1+\tilde{\omega}^2)^{1/2}/4(1+R^2)^{1/2}} \quad \text{(A4)}$$

Acknowledgments

The authors would like to thank James Bridges of NASA John H. Glenn Research Center at Lewis Field for providing the acoustic data shown in Fig. 6, as well as mean flow and turbulence data for the jets considered in this paper and his help in interpreting and using the data. Nicholas Georgiadis of NASA John H. Glenn Research Center at Lewis Field provided the corresponding RANS solutions. We thank Phillip Morris of Pennsylvania State University and Khairul Zaman of NASA John H. Glenn Research Center at Lewis Field for providing early results of their experimental measurements. Abbas Khavaran of Arctic Slope Research Corporation originally suggested the use of the WKBJ approximation introduced in Sec. III. S.J. Leib thanks E. Brian Fite of NASA John H. Glenn Research Center at Lewis Field for his support of this work. Support was also provided by the NASA Fundamental Aeronautics Program Supersonics Project.

References

[1] Lighthill, M. J., "On Sound Generated Aerodynamically: I. General Theory," *Proceedings of the Royal Society of London A*, Vol. 211, 1952, pp. 564–587.

[2] Lilley, G. M., "On the Noise from Jets," AGARD CP-131, 1974, pp. 13.1–13.12.

[3] Khavaran, A., Bridges, J., and Georgiadas, N., "Prediction of Turbulence-Generated Noise in Unheated Jets," NASA TM 2005-213827, 2005.

[4] Goldstein, M. E., and Leib, S. J., "The Aeroacoustics of Slowly Diverging Supersonic Jets," *Journal of Fluid Mechanics*, Vol. 600, 2008, pp. 291–337. doi:10.1017/S0022112008000311

[5] Goldstein, M. E., "A Generalized Acoustic Analogy," *Journal of Fluid Mechanics*, Vol. 488, 2003, pp. 315–333. doi:10.1017/S0022112003004890

[6] Harper–Bourne, M., "Jet Noise Turbulence Measurements," AIAA Paper 2003-3214, 2003.

[7] Morris, P. J., and Zaman, K. B. M. Q., "Velocity Measurements in Jets with Application to Noise Source Modeling," AIAA Paper No. 2009-17, 2009.

[8] Morris, P. J., and Zaman, K. B. M. Q., "Velocity Measurements in Jets with Application to Noise Source Modeling," *Journal of Sound and Vibration*, Vol. 329, No. 4, 2010, pp. 394–414. doi:10.1016/j.jsv.2009.09.024

[9] Morris, P. J., and Zaman, K. B. M. Q., "Two Component velocity Correlations in Jets and Noise Source Modeling," AIAA Paper No. 2010-3781, 2010.

[10] Bridges, J., and Brown, C. A., "Validation of the Small Hot Jet Rig for Jet Noise Research," AIAA Paper 2005-2846, 2005.

[11] Brown, C. A., and Bridges, J., "Small Hot Jet Acoustic Rig Validation," NASA TM-2006-214234, 2006.

[12] Bridges, J., and Wernet, M. P., "Measurements of the Aeroacoustic Sound Sources in Hot Jets," AIAA Paper 2003-3130, 2003.

[13] Bridges, J., and Wernet, M. P., "Effect of Temperature on Jet Velocity Spectra," AIAA Paper 2007-3628, 2007.

[14] Prokora, C. D., and McGuirk, J. J., "Spatio-Temporal Turbulence Correlation Using a High Speed PIV in an Axisymmetric Jet," AIAA Paper 3028-687, 2008.

[15] Afsar, M. Z., McGuirk, J. J., and Prokora, C. D., "Statistical Axi-Symmetry of the Two-Point Time-Delayed Reynolds Stress Autocovariance Tensor for Jet Noise Modeling," *Proceedings of the 19th Polish National Fluid Dynamics Conference*, Poznań, Poland, Sept. 2010.

[16] Afsar, M. Z., "The 'Two-Source' Structure of Jet Noise," Submitted to *European Journal of Mechanics/B Fluids*, 2011.

[17] Goldstein, M. E., and Rosenbaum, B. M., "Effect of Anisotropic Turbulence on Aerodynamic Noise," *Journal of the Acoustical Society of America*, Vol. 54, No. 3, 1973, pp. 630–645. doi:10.1121/1.1913643

[18] Khavaran, A., "Role of Anisotropy in Turbulent Mixing Noise," *AIAA Journal*, Vol. 37, No. 7, 1999, pp. 832–841. doi:10.2514/2.7531

[19] Goldstein, M. E., "The Low Frequency Sound from Multipole Sources in Axisymmetric Shear Flows with Application to Jet Noise," *Journal of Fluid Mechanics*, Vol. 70, No. 3, 2006, pp. 595–604. doi:10.1017/S0022112075002212

[20] Balsa, T. F. "The Acoustic Field of Sources in Shear Flow with Application to Jet Noise: Convective Amplification," *Journal of Fluid Mechanics*, Vol. 79, No. 01, 2006, pp. 33–47. doi:10.1017/S0022112077000020

[21] Afsar, M. Z., Dowling, A. P., and Karabasov, S. A., "Jet Noise in the Zone of Silence," AIAA Paper 2007-3606, 2007.

[22] Batchelor, G. K., *The Theory of Homogeneous Turbulence*, Cambridge Univ. Press, Cambridge, England, U.K., 1960, p. 179.

[23] Karabasov, S. A., Afsar, M. Z., Hanes, T. P., Dowling, A. P., McMullan, W. A., Pokora, C. D., Page, G. J., and McGuirk, J. J., "Using Large Eddy Simulation within an Acoustic Analogy Approach for Jet Noise Modeling," AIAA Paper 2008-2985, 2008.

[24] Karabasov, S. A., Afsar, M. Z., Hanes, T. P., Dowling, A. P., McMullan, W. A., Pokora, C. D., Page, G. J., and McGuirk, J. J. "Jet Noise: Acoustic Analogy Informed by Large Eddy Simulation," *AIAA Journal*, Vol. 48, No. 7, 2010, pp. 1312–1325. doi:10.2514/1.44689

[25] Wundrow, D. W., and Khavaran, A., "On the Applicability of High-Frequency Approximations to Lilley'S Equation," *Journal of Sound and Vibration*, Vol. 272, Nos. 3–5, 2004, pp. 793–830. doi:10.1016/S0022-460X(03)00420-6

[26] Tester, B. J., and Morfey, C. L., "Jet Mixing Noise: A Review of Single Stream Temperature Effects," AIAA Paper 2009-3376, 2009.

[27] Gradshteyn, I. S., and Ryzhik, I. M., *Table of Integrals, Series, and Products*, Academic Press, New York, 1965, p. 717.

[28] Morris, P. J., and Boluriaan, S., "The Prediction of Jet Noise from CFD data," AIAA Paper 2004-2977, 2004.

[29] Goldstein, M. E., "Ninety-Degree Acoustic Spectrum of a High-Speed Air Jet," *AIAA Journal*, Vol. 43, No. 1, 2005, pp. 96–102. doi:10.2514/1.9060

[30] Raizada, N., and Morris, P. J., "Prediction of Noise from High-Speed Subsonic Jets Using and Acoustic Analogy," AIAA Paper 2006-2596, 2006.

[31] McMullen, W. A., Pokora, C. D., Page, G. J., and McGuick, J. J., "Large Eddy Simulation of a High Reynolds Number Subsonic Turbulent Jet of Acoustic Source Capture," AIAA Paper 2008-2974, 2008.

[32] Viswanathan, K., "Best Practices for Accurate Measurement of Pure Jet Noise," *International Journal of Aeroacoustics*, Vol. 9, Nos. 1–2, 2010, pp. 145–206.

[33] Dahl, M. (ed.), "Assessment of NASA's Aircraft Noise Prediction Capability," NASA TP-2010-215653, To be Published.

[34] Morris, P. J., and Miller, S. A. E., "The Prediction of Broadband Shock-Associated Noise Using RANS CFD," AIAA Paper 2009-3315, 2009.

M. Glauser
Associate Editor